Chemical Engineering Journal 98 (2004) 183–198

Chemical Engineering Journal

www.elsevier.com/locate/cej

Multimonomer emulsion copolymerization in presence of inhibitors

M. Zubitur [a], S. Ben Amor [a], C. Bauer [b], B. Amram [b], M. Agnely [b], J.R. Leiza [a], J.M. Asua [a,*]

[a] *Facultad de Ciencias Químicas, Departamento de Química Aplicada, Institute for Polymer Materials (POLYMAT) and Grupo de Ingeniería Química, The University of the Basque Country, Apdo 1072, E-20080 Donostia-San Sebastián, Spain*

[b] *Rhodia, Centre de Recherches d'Aubervilliers, 52 rue de la Haie Coq, F-93308 Aubervilliers Cedex, France*

Received 10 March 2003; accepted 5 July 2003

Abstract

The comparison of the mathematical model and experimental results of the free radically initiated semi-continuous emulsion polymerization of styrene/butadiene/acrylic acid in the presence of chain transfer agent (CTA) is presented. The mathematical model takes into account the mechanism of gel formation and the effect of acidic monomers. It has also been included the inhibition caused by oxygen and monomer inhibitor. The experimental results (solids content, unreacted amount of monomer and gel content) and those obtained by the model are in rather good agreement.

Keywords: Emulsion polymerization; Mathematical modeling; Multimonomer system; Inhibition

1. Introduction

Emulsion polymerization is a free radical polymerization whose kinetics is severely affected by the presence of small amounts of inhibitors and retarders. These substances are polymerization supressors of different degrees of effectiveness [1]. Inhibitors completely stop the polymerization, whereas retarders are less efficient and cause only a reduction of the polymerization rate.

Kinetic studies in emulsion polymerization are often performed in the absence of inhibitors. The initiators and emulsifiers are of a high purity grade, and the monomers are purified by distillation to remove the inhibitors used during storage as well as other reactive organic impurities which may act as radical scavengers or chain transfer agents (CTAs). On the other hand, in industrial processes it is impractical to purify the monomers or at least to do so to the extent done in laboratory studies.

Oxygen is a well-known inhibitor for many free-radical polymerization systems. Initial rates of polymerization may be extremely low during the period in which molecular oxygen is acting as a retarder or an inhibitor. The action of oxygen as a radical scavenger (inhibitor) causing a decrease in the polymerization rates has been observed by several researchers. Nomura et al. [2] found that, in the presence of oxygen, the polymerization rate decreased when the agitation rate increased, namely when the oxygen mass transport rate from the headspace to the aqueous phase increased. Saenz and Asua [3] studied the effect of the nitrogen purge and monomer purification, on the particle-size distribution in the dispersion polymerization of styrene in ethanol. They found that the inhibitors contained in the technical monomers were less critical than oxygen because as they were completely dissolved in the reaction mixture, their main effect was to provoke a time delay in the start of the polymerization, whereas the diffusion of the oxygen from the headspace to the reaction mixture led to a continuous retardation. Vega et al. [4] noted that the presence of variable amounts of oxygen distorted the conversion profile in the emulsion copolymerization of acrylonitrile and butadiene carried out in an industrial reactor. Lopez de Arbina et al. [5] conducted a calorimetric study on the influence of oxygen on the seeded styrene emulsion polymerization. A decrease of the inhibition period and an increase of the polymerization rate was observed when the system is purged with nitrogen. They also found that oxygen had a great influence on the polymerization kinetics, producing not only inhibition, but also decreasing the reaction rate. The explanation for these results was the existence of mass transfer limitations from the reactor headspace to the latex, resulting in a gradual, continuous flow of oxygen into the liquid phase. Cunningham et al. [6] carried out measurements of oxygen initially dissolved in the aqueous phase in the styrene emulsion polymerization and show that oxygen was most appropriately treated as both water-soluble and

* Corresponding author. Fax: +34-943-212236.
E-mail address: jmasua@sq.ehu.es (J.M. Asua).

1385-8947/$ – see front matter © 2003 Elsevier B.V. All rights reserved.
doi:10.1016/S1385-8947(03)00185-2

Nomenclature

A	hydrophilic monomer
A_{gl}	gas–liquid surface area (dm^2)
d_p	diameter of a swollen particle (cm)
D_{Mw}	aqueous diffusion constant of monoradicals from monomer M (dm^2/s)
$D_{w(i)}$	average aqueous diffusion constant over all monomeric radicals of length i (dm^2/s)
[DB]	concentration of pendant double bonds in inactive polymer (mol/l)
$[DB]_t$	concentration of pendant double bonds in inactive and active polymer (mol/l)
E_{inhib}	activation energy (K^{-1})
f	initiator efficiency (–)
f_a	radical entry efficiency (–)
F_i	feed rate of monomer i (mol/s)
F_I	feed rate of initiator (mol/s)
F_{ox_m}	feed rate of the oxygen that enters in the reactor system with the monomer feed stream (mol/s)
F_{ox_w}	feed rate of the oxygen that enters in the reactor system with the water feed stream (mol/s)
F_t	feed rate of CTA (mol/s)
F_{TBC}	feed rate of TBC (mol/s)
G_1	amount of gel (–)
H_{O_2}	Henry's constant of oxygen (atm)
$[I_2]$	initiator concentration (mol/l)
k	mass transfer coefficient at the gas–liquid interface (dm/s)
k_a	average entry rate coefficient for all radicals (l/mol s)
$k_{a(i)}$	average entry rate coefficient for radicals containing i monomer units (l/mol s)
k_{fm}	average rate constant for transfer to monomer (l/mol s)
k_{ft}	average transfer rate constant for all radicals to chain transfer agent T (l/mol s)
k_{inhib}	pre-exponential factor of Eq. (15) (l/mol s)
k_I	initiator decomposition rate constant (s^{-1})
k_p	average rate constant for propagation in the particle phase (mol/l s)
k_{pw}	average rate constant over all radicals for propagation in the water phase (mol/l s)
k_p^*	average rate constant for propagation to pendant double bonds (mol/l s)
$\bar{k}_{pi}^z$	average rate constant for propagation to monomer i in phase z (l/mol s)
$k_{Rekker\,COOH}$	Rekker coefficient of acidic groups (–)
k_{tpo}	oxygen inhibition constant rate in the particle phase (l/mol s)
k_{twc}, k_{twd}	average constant over all radicals for aqueous termination by combination (l/mol s)
k_{two}	oxygen inhibition constant rate in the aqueous phase (l/mol s)
k_{TBC}	TBC inhibition constant rate (l/mol s)
m_{O_2}	number of moles of oxygen (mol)
m_{TBC}	TBC partition coefficient between droplets and particles (–)
m_w	number of moles of water (mol)
M_i	number of moles of monomer i in the reactor (mol)
$[M_i]_z$	concentration of an individual monomer M_i in phase z (mol/l)
$\bar{M}_{n,sol}$	number average molecular weight of the sol fraction (g/mol)
$\bar{M}_{w,sol}$	weight average molecular weight of the sol fraction (g/mol)
MW_w	water molecular weight (g/mol)
$\bar{n}$	average number of free radicals per particle (–)
n_A	number of monomers of type A (–)
n_S	number of monomers of type S (–)
N_A	Avogadro's number
N_p	number of polymer particles (–)
ox_i	oxygen concentration in the initial charge (mg/l)
ox_m	oxygen concentration in the monomer feed (mg/l)
O_2	total amount of oxygen in reaction medium (mol)
O_{2a}	oxygen in the headspace (mol)
$[O_2]_e$	concentration of oxygen in the reaction medium phase that would be in equilibrium with the oxygen concentration in the gas phase (mol/l)
$[O_2]_z$	oxygen concentration in phase z (p, monomer-swollen polymer particles; w, aqueous phase; d; monomer droplets) (mol/l)
p_{DB}	proportion of pendant double bonds in inactive polymer chains (–)
P_m	molecular weight of the monomeric unit (g/mol)
P_{Mw}	probability that of all oligoradicals in aqueous phase the end group is M (–)
P_{O_2}	partial pressure of oxygen (atm)

Q_j	jth moment of the inactive polymer distribution in the particle phase
$Q_j(n)$	jth moment of the inactive polymer distribution in generation n in the particle phase
$[R_w]$	concentration of all oligoradicals in the aqueous phase (mol/l)
S	hydrophobic monomer
T	CTA in the reactor (mol)
$[T]_p$	concentration of CTA (T) in polymer particles (mol/l)
TBC	TBC in the reactor (mol)
$[TBC]_z$	concentration of TBC in phase z (p, monomer-swollen polymer particles; d; monomer droplets) (mol/l)
V_z	volume of phase z (p, monomer-swollen polymer particles; w, aqueous phase; d; monomer droplets) (l)
X_{O_2}	molar fraction of oxygen
Y_j	jth moment of the polymeric radical distribution in the particle phase
$Y_j(n)$	jth moment of the polymeric radical distribution in generation n in the particle phase

Greek symbols

β_1	oxygen partition coefficient between water and particles
β_2	oxygen partition coefficient between water and droplets
ρ_w	water density (g/l)

monomer-soluble inhibitor. They found that at high initial oxygen levels low molecular weight was produced. This effect is an indicator that the oxygen remains in the organic phase. On the other hand they found an exponential dependence of induction time on initial oxygen concentration that provided evidence for slow diffusion of oxygen from the headspace into the latex. If there were no diffusion from the headspace, a linear relationship will be observed between the initial oxygen concentration and induction time.

Huo et al. [7] studied the effect of water-soluble and monomer-soluble impurities on the kinetics of emulsion polymerization of monomers following Case II kinetics (e.g. styrene) in a batch reactor. They modified the mathematical model presented by Broadhead et al. [8] by modifying the radical balances in the reactor to include reactions with water-soluble (hydroquinone) and monomer-soluble (*tert*-butylcatechol) impurities. Their experimental studies reveal that impurities can have an appreciable effect on both polymer nucleation and growth. These effects were accounted for by a mathematical model.

Penlidis et al. [9] investigated the effect of water-soluble and monomer-soluble impurities on the kinetics of emulsion polymerization for Case I systems (e.g. vinyl acetate). They modified a population balance model for Case I emulsion polymerizations developed by Penlidis et al. [10], to account for the effects of impurities. The model was able to account for the experimentally found induction period that was proportional to the amount of impurities present.

Chien and Penlidis [11,12] studied the effect of the impurities on a continuous methyl methacrylate solution polymerization reactor system. The inhibitor used in the experiments was 2-2-diphenyl-1-picrylhydrazil (DPPH). In the open loop experiments [11] they compared the results with model predictions and found that conversion data agreed well, but larger discrepancies were found for average molecular weight. On the hand, closed-loop control strategies [12] were performed to keep the conversion at the desired level while adding known and unknown disturbances of impurities to the process. Different controllers were assessed by simulation and real-time experiments and in all cases the conversion was controlled in the nominal value.

Recently, Kiparissides et al. [13] developed a mathematical model to quantify the effect of the oxygen concentration on the polymerization rate and particle size distribution in *ab initio* vinyl chloride batch emulsion polymerization reactor. They found that, at low initial oxygen concentrations, the polymerization rate increases with the oxygen concentration and that the average latex particle size exhibits a U-shaped behavior with respect to the initial oxygen concentration. They explain this experimental observation by the combined role of oxygen as an inhibitor and a radical generator through the formation and subsequent decomposition of vinyl peroxides formed via the copolymerization of vinyl chloride with oxygen.

In a previous paper [14] a mathematical modeling of a semi-continuous emulsion polymerization of a multimonomer system comprising vinylic, divynilic, and water-soluble monomers in the presence of CTA was presented. In this work, the model is extended to account for the effect of impurities in the monomer feedstock and the presence of oxygen in the monomer and reactor headspace. These inhibitors might affect the kinetics of the emulsion polymerization but also in the structural properties of the polymer latex (MWD and gel). In this paper the predictions of the extended model are compared with experimental data (solids content, unreacted amount of monomer and gel content) of the seeded semi-batch emulsion polymerization of styrene (S)/butadiene (Bd)/acrylic acid (AA). The commercial importance of all the above properties for a latex makes such a model useful for the design, optimization, and control of emulsion polymerization reactors.

2. Experimental

Data were gathered using an on-line Raman Spectrometer (Bruker RFS 1000) [15] in a 5 l reactor, that allowed the measurement of the solids content and free styrene every

Table 1
Basic formulation used in the experiments

	Initial charge (g)	Feed[a] (g)
Prepolymerized latex	6.7	–
S	–	1152
Bd	–	580
AA	–	37.4
CTA (*tert*-dodecyl mercaptan)	–	11.16
Anionic surfactant	–	9.18
Initiator (ammonium persulfate)	–	15.5
Water	1500	260.82

[a] Feeding time 4.5 h in all the experiments.

6 min. In addition to these measurements, for several experiments the final amount of gel produced was also measured. The experimental procedure was as follows: a prepolymerized latex and a part of water were initially charged into the reactor. The rest was fed divided in two streams having both the same total feeding time: one was composed by monomers and CTA and the other was the initiator and emulsifier in aqueous solution. The basic formulation is shown in Table 1. The purging procedure was as follows: the system was vacuum down to 0.1 bar, then it was purged with nitrogen to atmospheric pressure and again vacuum down to 0.1 bar. The system was heated to the reaction temperature (heating period 50 min) and the reagent feeding was started ($t = 0$). The operating pressure was 4–6 bar during the feeding period and then decreased to 1–2 bar.

In addition to the on-line measurements of solids content and unreacted styrene measured by FT-Raman spectroscopy, off-line analysis were performed. The solids content (defined as the dry latex weight/wet latex weight ratio) was measured by gravimetry. Styrene concentration (defined as weight styrene per weight of wet latex) was measured by GC. Both off-line and on-line measurements were in good agreement [15]. The process variables varied during this study were: styrene/butadiene ratio, reaction temperature and CTA concentration as it is shown in Table 2.

Table 2
Semi-continuous experiments carried out with different temperatures, S/Bd ratios and CTA concentrations

Run[a]	Temperature (°C)	S/Bd	CTA[b]
1	85	2.0	0.89
2	85	2.0	0.89
3	80	2.0	0.89
4	90	2.0	0.89
5	85	2.0	0.66
6	85	2.0	0.66
7	90–85	2.5	1.67
8	90–80	2.5	1.67
9	90	2.5	1.67
10	95	2.0	1.56
11	95	2.0	1.46

[a] Runs 1–6 contained oxygen in the initial charge. Runs 7–11 did not contain oxygen in the initial charge.
[b] wt.% with respect to the monomers.

3. Mathematical model

3.1. Outline and assumptions

A mathematical model developed in a previous work [14] for the semi-continuous emulsion polymerization of a system comprising vinylic, divinylic and water-soluble monomers in the presence of CTA was extended to take into account the presence of inhibitors. For the sake of brevity in what follows, only the distinctive kinetics aspects of the polymerization in the presence of inhibitors will be described and discussed. The material balances and molecular weight distribution are given in Appendices A and B. A complete description of the mathematical model can be found in Ref. [14].

Inhibition is a consequence of the presence of impurities (e.g., the inhibitors in the monomer feed stream and oxygen traces in the nitrogen atmosphere of the reactor and in the feed streams). The inhibitors consume the free radicals produced by decomposition of the initiator leading to an inhibition period, and hence to an increase in the amount of free monomers.

3.2. Reaction scheme

Oxygen diffuses from the gas phase into the reaction medium where it reacts with free radicals in aqueous phase ($R^\bullet$) and in particles ($R_m^\bullet$) according to the following kinetic mechanism:

$$R^\bullet\,(aq) + O_2\,(aq) \xrightarrow{k_{two}} RO_2^\bullet\,(aq) \quad \text{(inactive)}$$

$$R_m^\bullet + O_2(p) \xrightarrow{k_{tpo}} RO_2^\bullet(p) \quad \text{(inactive)}$$

The inactive radicals $RO_2^\bullet$ were considered in the mathematical model as dead polymer.

Radicals in particles may also react with monomer-soluble impurities such as *tert*-butylcatechol (TBC), which are commonly added to the fresh monomer by the suppliers due to their radical scavenging properties

$$R_m^\bullet + TBC(p) \xrightarrow{k_{TBC}} P_m(TBC)$$

The use of k_{two}, k_{tpo} and k_{TBC} as overall rate constant, regardless of the monomer reactivity with the impurity is a simplification to the model.

3.3. Material balances

3.3.1. Oxygen

Oxygen in the headspace diffuses to the reaction mixture according to the following balance:

$$\frac{dO_{2a}}{dt} = -kA_{gl}([O_2]_e - [O_2]_w) \quad (1)$$

where O_{2a} (mol) is the total amount of oxygen in the headspace, k (dm^3 phase/dm^2 s = dm/s) is the mass

transfer coefficient at the gas–liquid interface, A_{gl} (dm^2) is the gas–liquid interfacial area, $[O_2]_e$ (mol/l) is the concentration of oxygen in the aqueous phase that would be in equilibrium with the concentration of oxygen in the gas phase and $[O_2]_w$ (mol/l) is the oxygen concentration in aqueous phase.

The material balance for oxygen in the reaction medium is given by the following equation:

$$\frac{dO_2}{dt} = F_{ox_w} + F_{ox_m} + kA_{gl}([O_2]_e - [O_2]_w) - k_{two}[R_w][O_2]_w V_w - k_{tpo}\frac{\bar{n}N_p}{N_A}[O_2]_p \quad (2)$$

where O_2 (mol) is the total amount of oxygen in latex, F_{ox_w} (mol/s) is the feed rate of the oxygen that enters in the reactor system with the water feed stream, F_{ox_m} (mol/s) is the feed rate of the oxygen that enters in the reactor system with the monomer feed stream. The third term of the right-hand side accounts for transfer of oxygen from the gas phase to the latex phase and the fourth and fifth account for the consumption of oxygen by radicals in the aqueous and polymer particles phases, respectively. k_{two} and k_{tpo} (l/mol s) are the oxygen inhibition rate constants in aqueous phase and in particles, respectively, $[R_w]$ (mol/l) is the concentrations of radicals in the aqueous phase, V_w (l) is the volume of the aqueous phase, $\bar{n}$ is the average number of free radicals per particle, N_p is the total number of polymer particles in the reactor, N_A is the Avogadro's number, and $[O_2]_p$ (mol/l) is the oxygen concentration in particles.

3.3.2. Monomer inhibitor (TBC)

TBC is too insoluble to be present in the aqueous phase, hence its mass balance is

$$\frac{dTBC}{dt} = F_{TBC} - k_{TBC}[TBC]_p\frac{\bar{n}N_p}{N_A} \quad (3)$$

where TBC is the total number of moles of TBC in the reactor, F_{TBC} (mol/s) is the feed rate of TBC, k_{TBC} (l/mol s) is the TBC inhibition constant rate, and $[TBC]_p$ (mol/l) is the concentration of TBC in the polymer particles.

3.4. Inhibitors distribution between the phases

3.4.1. Oxygen

The total amount of oxygen in the reaction medium is the sum of the oxygen in the aqueous phase, polymer particles and droplets (if present):

$$O_2 = [O_2]_w V_w + [O_2]_p V_p + [O_2]_d V_d \quad (4)$$

where $[O_2]_d$ (mol/l) is the oxygen concentration in droplets, V_d and V_p (l) are the volumes of droplets and particles, respectively. The relationship between oxygen in water and oxygen in particles and in droplets is given by partition coefficients (β_1 and β_2, respectively):

$$[O_2]_p = \frac{[O_2]_w}{\beta_1} \quad (5)$$

$$[O_2]_d = \frac{[O_2]_w}{\beta_2} \quad (6)$$

The concentration of oxygen in the aqueous phase that would be in equilibrium with the oxygen concentration in the gas phase, $[O_2]_e$, is given by Henry's Law:

$$P_{O_2} = H_{O_2} X_{O_2} \quad (7)$$

where P_{O_2} (atm) is the partial pressure of oxygen, H_{O_2} (atm) is the Henry's constant of oxygen and X_{O_2} is the molar fraction of oxygen. Eq. (7) has been modified as:

$$P_{O_2} = H_{O_2}\frac{m_{O_2}}{m_{O_2} + m_w} \approx H_{O_2}[O_2]_e\frac{MW_w}{\rho_w} \quad (8)$$

where m_{O_2} and m_w are the number of moles of oxygen and water, respectively, MW_w is the water molecular weight (g/mol) and ρ_w is the water density (g/l).

3.4.2. TBC

The total amount of TBC is given by the following equation:

$$TBC = [TBC]_p V_p + [TBC]_d V_d \quad (9)$$

where $[TBC]_p$ and $[TBC]_d$ are the concentrations of TBC in particles and droplets, respectively. The concentration of

Table 3
Values of parameters used for the model predictions

Parameter		
k_p (l/mol s)	$4.27 \times 10^7\, e^{-3910/Temp}$ [16] (S-type)	$8.05 \times 10^7\, e^{-4271/Temp}$ [17] (Bd)
k_p (l/mol s)	$5 \times 10^8\, e^{-3560/Temp}$ [18] (A-type, associated form)	$2 \times 10^7\, e^{-3560/Temp}$ [18] (A-type, dissociated form)
k_{fm} (l/mol s)	3.35×10^{-5} [19] (S-type)	6.10×10^{-5} [20] (Bd)
k_{fm} (l/mol s)	1×10^{-5} [18] (A-type, associated form)	1×10^{-5} [18] (A-type, associated form)
$k_{twc} = k_{twd}$ (l/mol s)	1×10^8 [18] (S-type)	1×10^8 [18] (Bd)
$k_{twc} = k_{twd}$ (l/mol s)	1×10^8 [18] (A-type, associated form)	1×10^8 [18] (A-type, associated form)
k_p/k_p^*	300 [18]	
f	0.6	
β_1	0.4 [21]	
β_2	0.83 [21]	
k_{TBC} (l/mol s)	1.0×10^5 [21]	
m_{TBC}	1.5 [21]	

TBC in the polymer particle is

$$[\mathrm{TBC}]_\mathrm{p} = \frac{\mathrm{TBC}}{V_\mathrm{p} + V_\mathrm{d} m_\mathrm{TBC}} \quad (10)$$

where m_TBC is the TBC partition coefficient between monomer droplets and particles.

The mathematical model described above and in Appendices A and B contains numerous parameters. Some of them are available in the literature (see Table 3). The concentrations of TBC in styrene (12 ppm) and TBC in butadiene (150 ppm) were provided by the monomer suppliers. The amount of oxygen in the water feed was measured as 5.0 mg/l.

Others parameters were not available or the range of parameters reported in the literature is very broad. Therefore, these parameters were estimated by fitting model predictions to the experimental data gathered in seeded semi-continuous emulsion polymerization of S/Bd/AA, namely: (i) the evolution of the solids content, (ii) the amount of free styrene and (iii) gel content.

The estimation was carried out using the Nelder and Mead algorithm [22] of direct search (DBCPOL subroutine, IMSL library) to minimize the following objective function:

$$J = \sum_{i=1}^{m}\sum_{j=1}^{n}\sum_{h=1}^{3}(y_{h\,\mathrm{exp}}(t) - y_{h\,\mathrm{the}}(t))^2 \quad (11)$$

where m is the number of experiments, n is the number of experimental points of each experiment, h is the number of variables (solids content, unreacted styrene and gel content), $y_{h\,\mathrm{exp}}(t)$ the experimental measurements of solids content, amount of unreacted styrene and gel content, and $y_{h\,\mathrm{the}}(t)$ are the theoretical predictions of these variables.

Table 4
Values of estimated parameters

Parameter	Value
k_inhib (l/mol s)	6.22×10^{13}
E_inhib (K^{-1})	6428
k (dm/s)	0.039
$k_\mathrm{Rekker\,COOH}$	−0.5
f_a	9.9×10^{-4}
$\mathrm{Ox_i}$ (mg/l)	0.30
$\mathrm{Ox_m}$ (ppm)	18.0

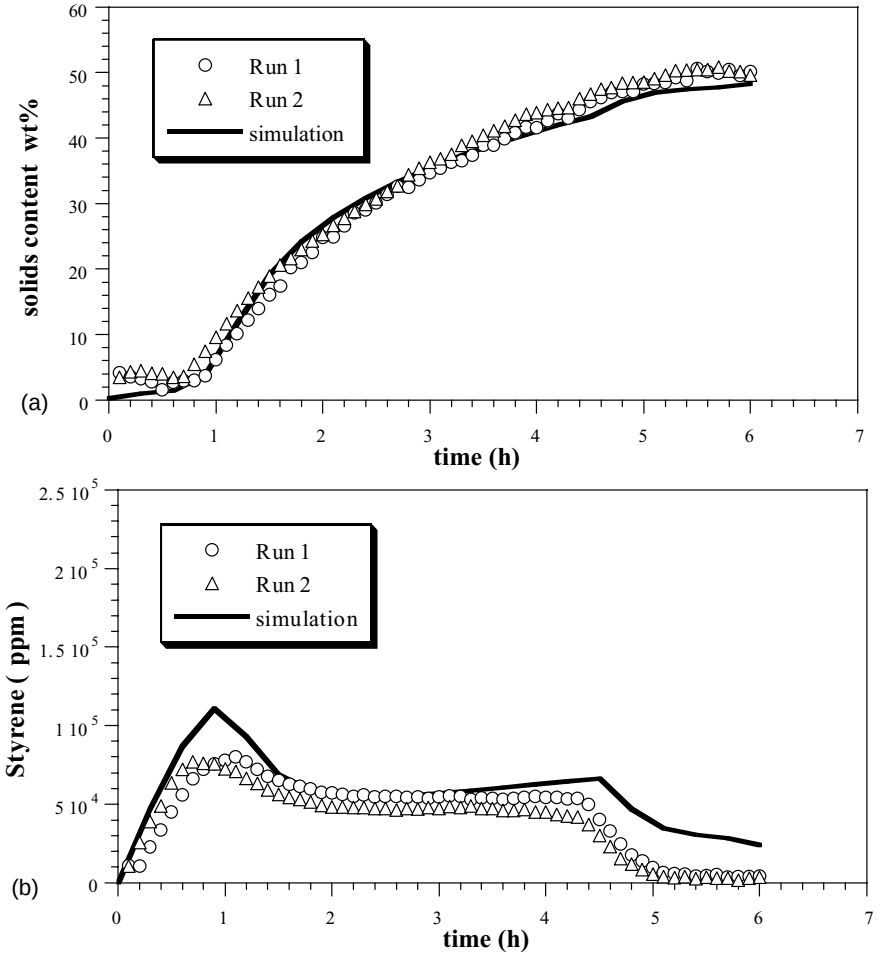

Fig. 1. Comparison between experimental and model simulations of (a) solids content and (b) amount of free styrene for Runs 1 and 2 ($T = 85\,^\circ\mathrm{C}$).

The adjustable parameters were as follows:

(i) Radical entry was assumed to occur by diffusion, and hence the average entry rate coefficient $k_{a(i)}$ (l/mol s) of any radical was calculated according to the Smoluchowski equation [23]:

$$k_{a(i)} = 2 \times 10^{-7} \pi f_a D_{w(i)} d_p N_A \quad (12)$$

where f_a is the particle entry efficiency factor, which was taken as adjustable parameter

$$D_{w(i)} = \frac{D_{w(1)}}{i^{1/2}} \quad (13)$$

$$D_{w(1)} = \sum_{M}^{n_A+n_S} p_{Mw} D_{Mw} \quad (14)$$

where $D_{w(i)}$ is the average diffusion coefficient (dm^2/s) of an oligoradical of length i in water, D_{Mw} is the diffusion coefficient of monomer M in water and p_{Mw} is the probability that of all oligoradicals in aqueous phase the end group is M.

(ii) The mass transfer coefficient at the gas–liquid interface, k (dm/s).

(iii) The Arrhenius dependence of the oxygen inhibition constant:

$$k_{tpo} = k_{two} = k_{inhib} \exp\left(-\frac{E_{inhib}}{T}\right) \quad (15)$$

where the pre-exponential factor k_{inhib} (l/mol s) and its dependency with temperature, the activation energy E_{inhib} (K^{-1}), were taken as adjustable parameters. The range of values of k_{tpo} found in the literature was: 1×10^6 to 1×10^7 l/mol s [24].

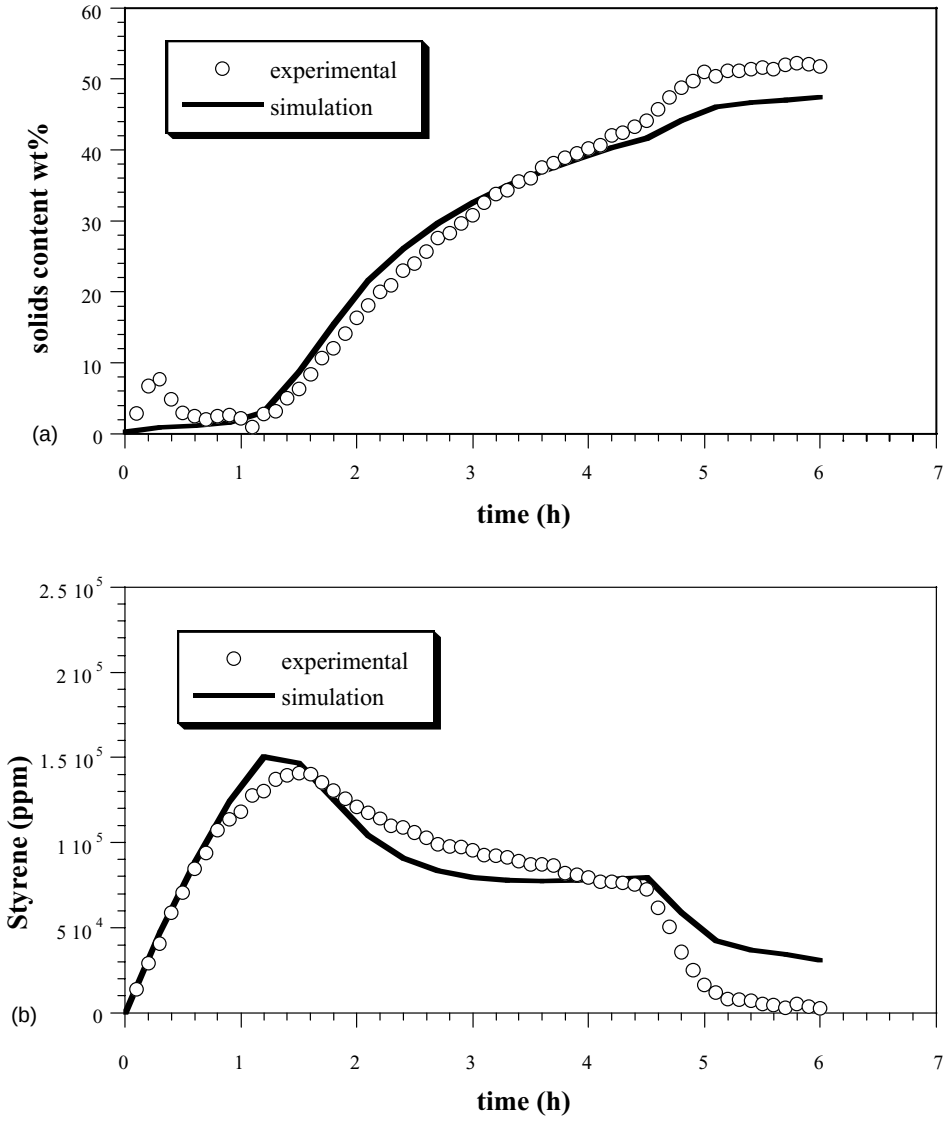

Fig. 2. Comparison between experimental values and model simulations of (a) solids content and (b) amount of free styrene for Run 3 ($T = 80\,^{\circ}C$).

(iv) The Rekker coefficient of acidic groups, $k_{\text{Rekker COOH}}$.
(v) The oxygen concentration in the initial charge, ox_i (mg/l) (only for reactions that shows an inhibition period at the start of the reaction, namely Runs 1–6) and the oxygen concentration in the monomer feed, ox_m. The experimental range for ox_i was 0.5–1.2 mg/l.

In order to fit the parameters, all the reactions shown in Table 2 were used. Table 4 presents the values of the parameters estimated in this work.

4. Results and discussion

4.1. Reactions with oxygen in the initial charge

In Runs 1–6 inhibition was observed after the monomer addition was started (Figs. 1–4). These experimental results showed the necessity of taking into account the inhibition in order to obtain a reliable model for the prediction of the emulsion polymerization of S/Bd/AA.

Runs 1 and 2 are replicated experiments carried out at 85 °C. Fig. 1a shows the comparison between the model predicted and experimental solids content, and Fig. 1b that of the free styrene. Fig. 1 shows that the process was reproducible. It can be observed that the model captured the main trends observed experimentally, in particular, it is noticeable the ability to predict the inhibition period.

In Runs 3 and 4 the temperature was varied. The other process variables were kept constant as presented in Table 2. Figs. 2 and 3 show the model predictions and the experimental results for Runs 3 and 4, respectively. Experimental results show that the inhibition period as well as the amount of free styrene decrease with increasing temperature. This effect was basically due to the increase of the rate constant for oxygen consumption with the temperature. The oxygen water solubility is inversely proportional to the temperature, hence, Henry's constant (Eq. (7)) increases with the temperature but the slope of this increase is very

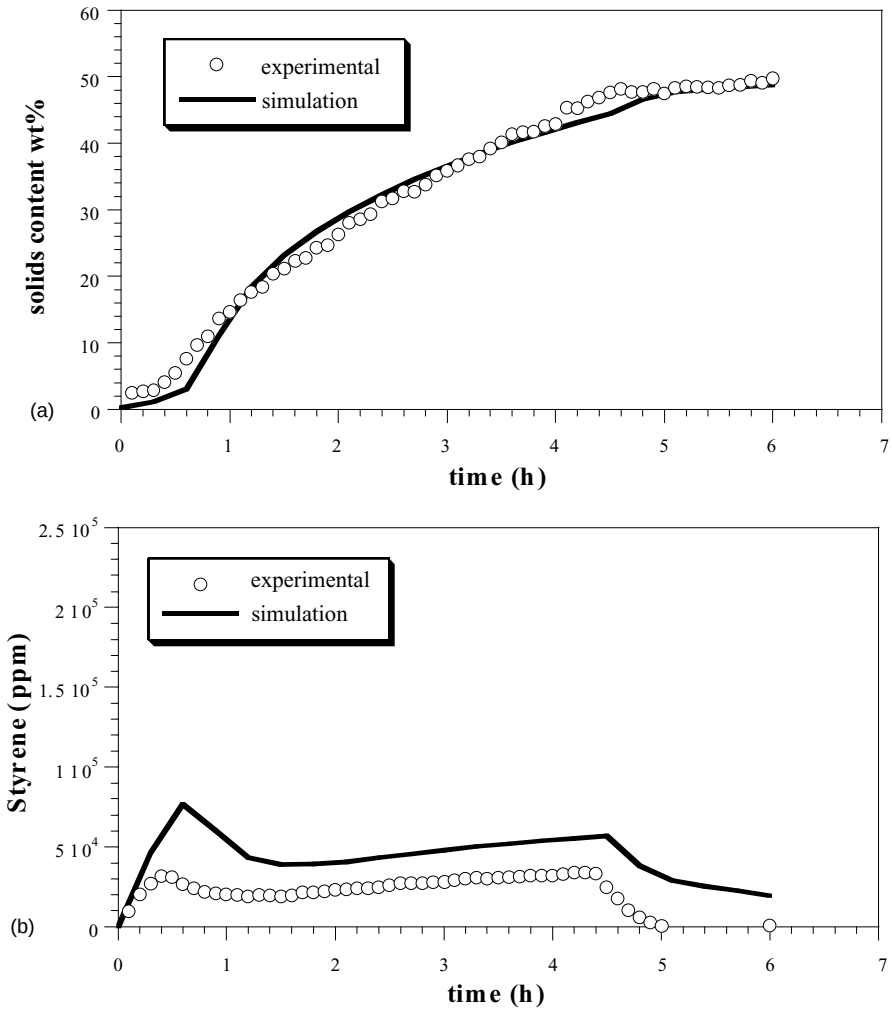

Fig. 3. Comparison between experimental values and model simulations of (a) solids content and (b) amount of free styrene for Run 4 ($T = 90$ °C).

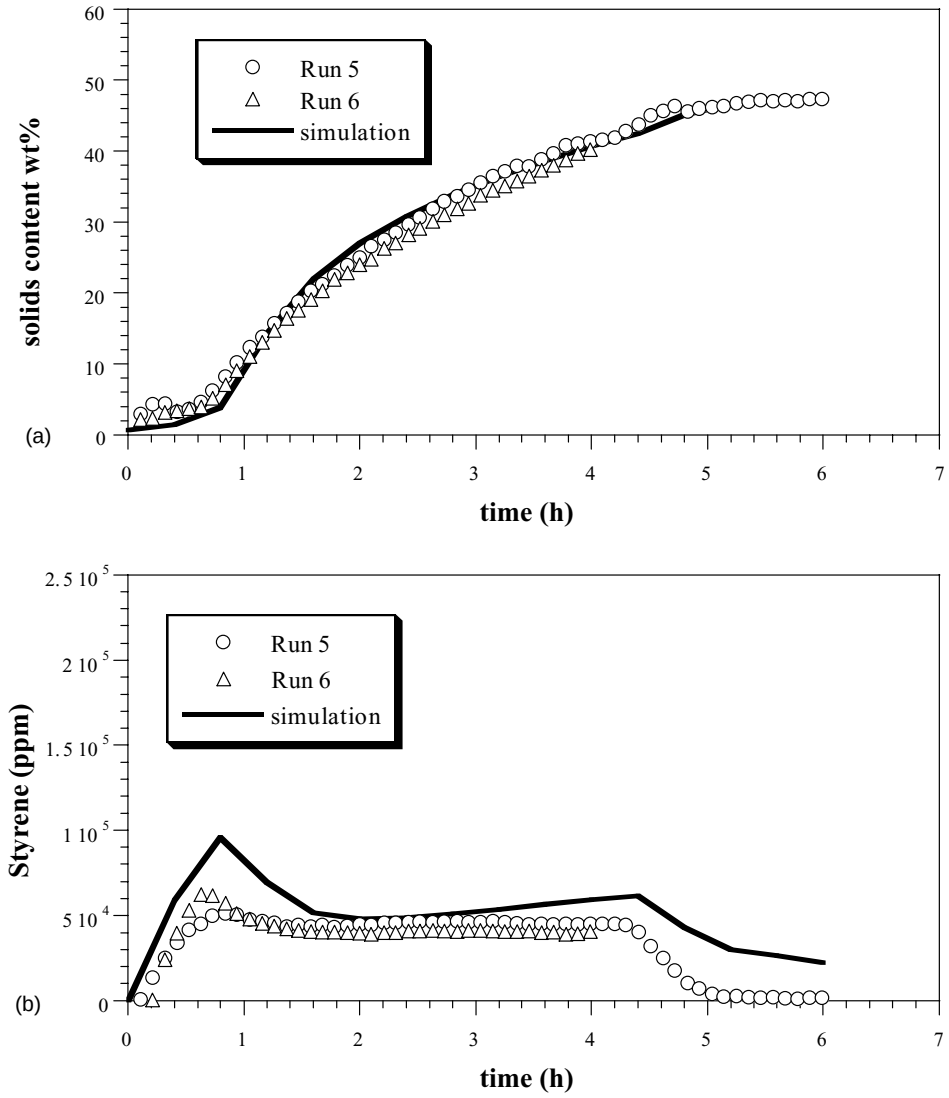

Fig. 4. Comparison between experimental values and model simulations of (a) solids content and (b) amount of free styrene for Runs 5 and 6 ($T = 85\,^{\circ}C$).

small in the temperature range 80–100 °C and H is approximately constant [25]. Therefore, the diffusion of oxygen from the headspace to the reaction medium did not change, whereas the oxygen consumption rate increased with temperature leading to a reduction of the inhibition period. Furthermore, the amount of free styrene decreased because of the increase of the polymerization rate (both propagation rate constant and radical concentration) with temperature. The mathematical model was able to simulate reasonably well this effect of the temperature on the extension of the inhibition period, as it is shown in Figs. 1–3 where both the predictions of the solids content and free styrene are shown.

Fig. 4 shows the solids content and free styrene time plots for two replicated experiments (Runs 5 and 6) carried out at the same temperature than Runs 1 and 2 but with a lower concentration of CTA (see Table 2). In Runs 1 and 2 the concentration of CTA was 0.89 wt.% (with respect to the monomers) and 0.66 wt.% in Runs 5 and 6. Fig. 4 displays a good reproducibility of the experiments and a good agreement between experimental data and model predictions for the inhibition period, the evolution of the solids content and the amount of free styrene.

Table 5 shows the comparison between experimental values and model predictions of the final gel content of the latexes. It can be seen that an increase of reaction temperature led to an increase of the amount of gel. The model predicted well this effect, which was due to the decrease in the effect of the inhibitors with the temperature. The inhibitors consume reactive-free radicals in the reactor, thereby preventing polymer from growing further and resulting in the reduction of the gel content. Increasing the temperature led to an increase to the oxygen consumption rate, decreasing the induction period and allowing to the radicals to grow further and propagate to the pendant double bonds increasing the gel fraction.

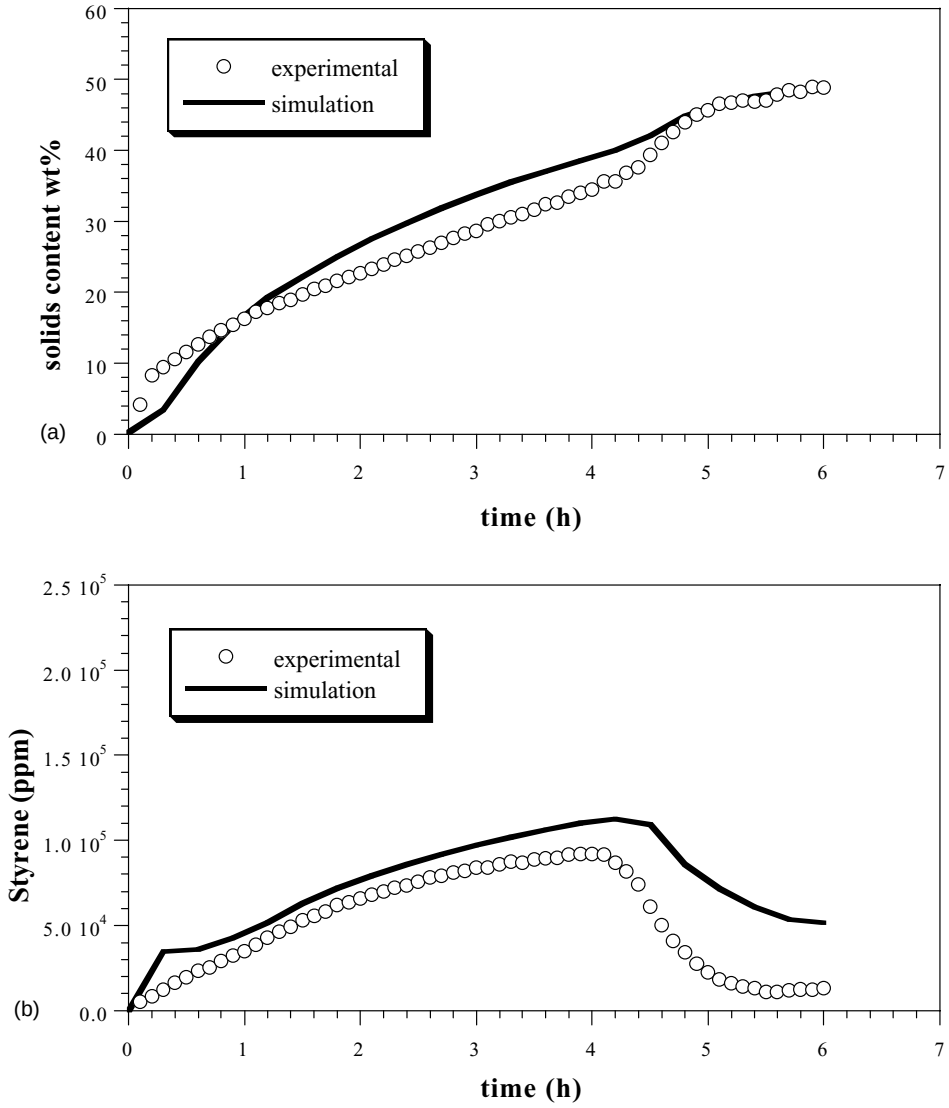

Fig. 5. Comparison between experimental values and model simulations of (a) solids content and (b) amount of free styrene for Run 7 ($T = 90$–$85\,^{\circ}C$).

Table 5
Comparison between experimental values and model prediction of the final gel content for the experiments

Run	Gel experimental (%)	Gel simulated (%)
1	64	67
2	69	67
3	55	49
4	73	76
5	Not measured	71
6	Not measured	71
7	Not measured	4.4×10^{-5}
8	2	4.9×10^{-5}
9	5	1.9×10^{-4}
10	24	27
11	20	34

4.2. Reactions without oxygen in the initial charge

For the second set of experiments, Runs 7–11 the reaction system was purged more efficiently (see Section 2) and no inhibition period was observed. In these reactions, the initial oxygen content was considered equal to zero.

Figs. 5–7 show the comparison of experimental data with model predictions for the solids content and unreacted amount of styrene for Runs 7–9. Runs 7–9 were carried out with a relatively high S/Bd ratio (S/Bd = 2.5) and a high concentration of CTA (1.67 wt.%). Moreover, Run 9 was carried out at a constant reaction temperature ($T = 90\,^{\circ}C$), whereas Runs 7 and 8 do have ramps down during the feeding period in the temperature range 90–85 and 90–80 °C, respectively. In these experiments no inhibition was observed. As expected, the polymerization rate increased with the temperature. The shape of the unreacted amount of styrene is different with respect to Runs 1–5, where there was oxy-

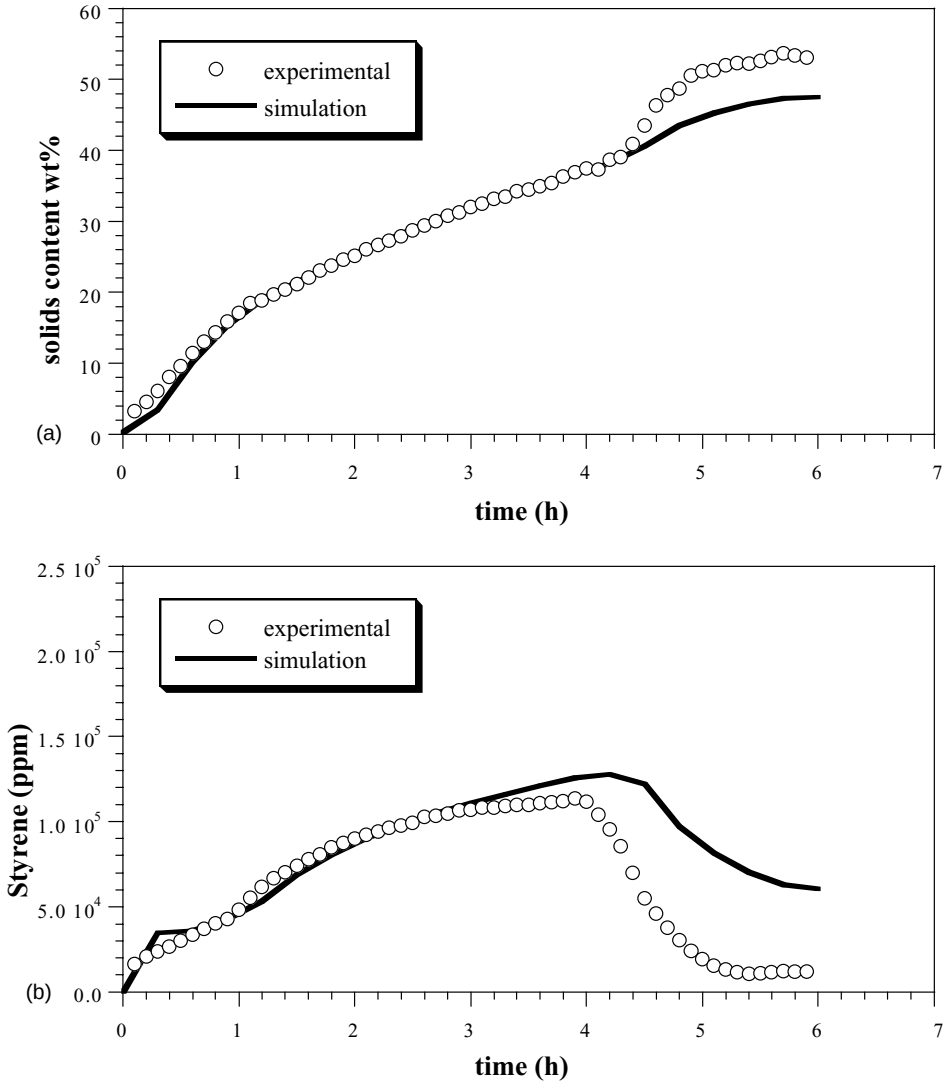

Fig. 6. Comparison between experimental values and model simulations of (a) solids content and (b) amount of free styrene for Run 8 ($T = 90$–$80\,^{\circ}C$).

gen in the initial stage of the process. In Runs 7–9, the amount of free styrene increased to a maximum value corresponding to the end of the feeding time and then decreased during the batch period. In general, model predictions compared well with experimental results, the fitting being better for the solids content than for the amount of free styrene, for which the prediction by the model was higher than that observed experimentally. This effect was also observed in the reaction carried out at the highest temperature of the previous set (Run 4). Since for these reactions the solids content measured experimentally and those obtained by the model are in rather good agreement, the deviation can be caused by: (i) diffusional limitations of butadiene from the gas phase to the latex phase that were not accounted by the model or (ii) incorrect partition coefficients or reactivity ratios used as parameters in the model. We were confident with data used for the partition coefficients and reactivity ratios taken from [26]. Thus, the former reason is likely the most important one. To check this point, simulations were carried out (not shown) decreasing the amount of butadiene in the polymer particle using a lower reactivity ratio for butadiene and allowing a larger consumption of styrene. This was done by assuming that the butadiene reactivity ratio was an additional parameter to be fitted. The agreement of the predicted unreacted amount of styrene with experimental results improved with respect to those shown in Figs. 5–7. This showed that a smaller amount of butadiene in the polymer particles may provide better predictions of the free styrene.

Table 5 shows that the amount of gel in Runs 7–9 is very small because less butadiene which limited crosslinking and more CTA which lowers the kinetic chain length were used in these experiments. On the other hand, less gel was produced in experiments carried out at lower temperatures because of the higher concentration of monomer in the polymer particles, which favored linear propagation to monomer over propagation to pendant double bonds (PDB) in inactive polymer.

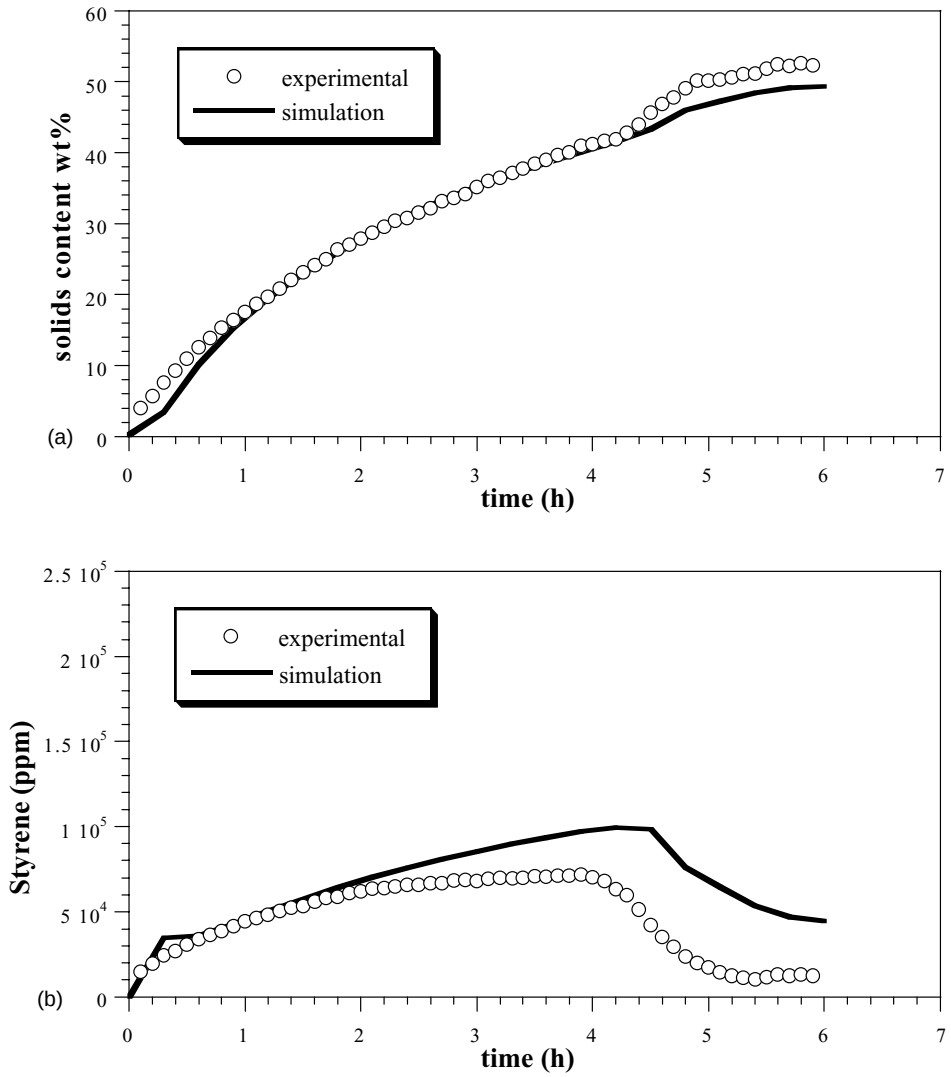

Fig. 7. Comparison between experimental values and model simulations of (a) solids content and (b) amount of free styrene Run 9 ($T = 90\,^{\circ}$C).

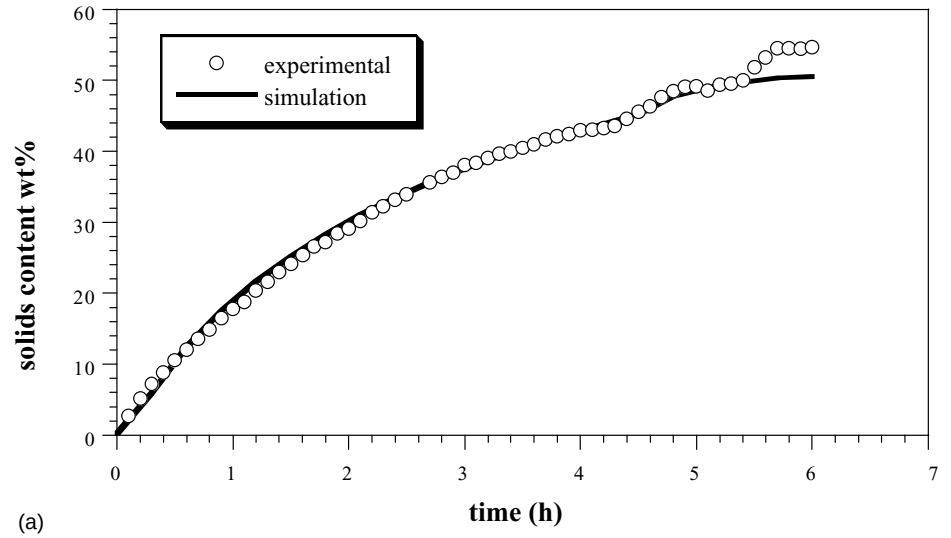

Fig. 8. Comparison between experimental values and model simulations of (a) solids content and (b) amount of free styrene for Run 10 ($T = 95\,^{\circ}$C).

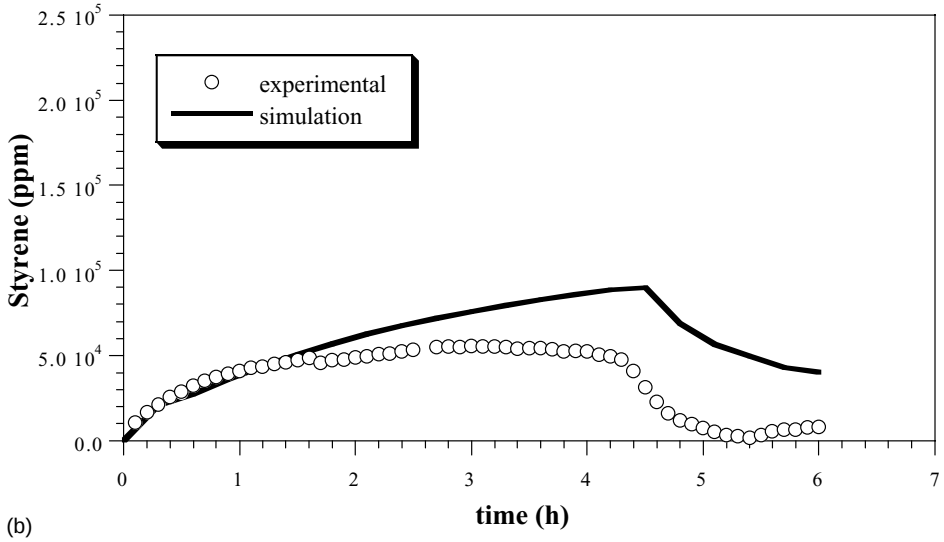

Fig. 8. (*Continued*).

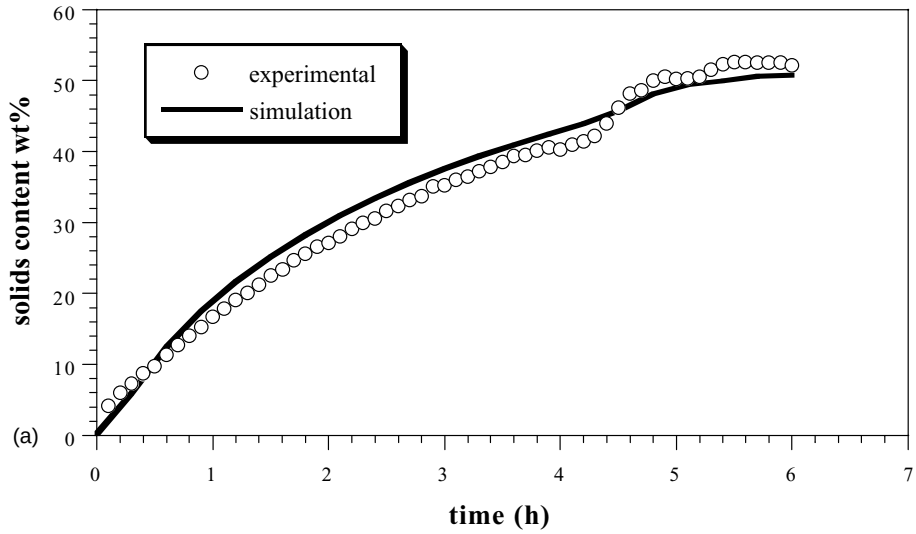

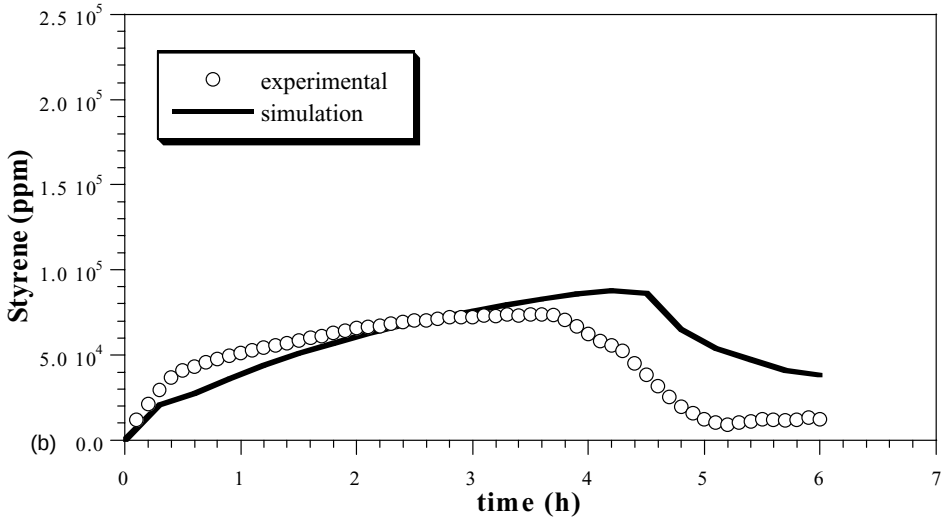

Fig. 9. Comparison between experimental values and model simulations of (a) solids content and (b) amount of free styrene for Run 11 ($T = 95\,^{\circ}\mathrm{C}$).

Figs. 8 and 9 show the comparison of experimental data and model predictions for the solids content and unreacted amount of styrene for Runs 10 and 11. These experiments were carried out at 95 °C with a S/Bd ratio of 2 and different amounts of CTA as shown in Table 2. The figure shows a reasonable agreement between model predictions and experimental results. The chain transfer reaction to CTA (*tert*-dodecyl mercaptan) is very fast and the CTA radicals formed react quickly with free monomer units. This means that it should not be any effect of the amount of CTA in the kinetic of the process and the predictions of the model do not show any difference in solids content or amount of free styrene between Runs 10 and 11.

Table 5 compares the experimental and simulated values of the gel content for Runs 10 and 11. The model predicts that the larger the CTA content the lower the gel content, because the chain transfer to CTA reduces the kinetic length. However, the experimental results do not show this trend although are quite similar (within the experimental error of the measurement). The explanation for this result is that in this system the gel amount is mainly controlled by the S/Bd ratio and the effect of changing this ratio is higher than the change of the amount of CTA. This effect can be observed comparing the gel content of Runs 7–9 (with S/Bd = 2.5) and Runs 10–11 (with S/Bd = 2).

5. Conclusions

A previously developed mathematical model for the semi-continuous emulsion polymerization of a vinylic, divinylic and acrylic acid type monomers was extended to account for inhibition caused by both oxygen and inhibitor contained in the monomer feed streams, and assessed with experimental results of a copolymerization system composed by styrene, butadiene and acrylic acid. The experiments were performed at high solids content (50 wt.%) under a wide range of experimental conditions.

Model simulations predicted reasonable well the evolution of the solids content, the unreacted amount of styrene and the final amount of gel. The model captured well the inhibition period observed in the experiments that contained oxygen in the initial charge and explained the decrease of the induction period decrease obtained by increasing the reaction temperature. The increase of the temperature led to an increase of the rate constant for oxygen consumption leading to a reduction of the inhibition period.

Some discrepancies were found between the predicted and measured unreacted amounts of styrene in the reactions carried out with absence of oxygen in the initial charge and they were attributed to a diffusional limitation of the butadiene from the headspace to polymer particle, which was not accounted for by the model.

The amount of gel formed was well predicted under the very wide range of conditions employed in the experiments. The good agreement between theoretical results and experimental measurements will allow to tailor formulations and feed policies to produce copolymer latexes with the desired structural properties for a particular use. In addition, it would be very useful for optimization and process control of the semi-batch emulsion polymerization of systems comprised by vinylic/divinylic/acrylic acid monomers.

Acknowledgements

The permission by Rhodia and Latexia to publish this work is appreciated. The financial support from the European Community to the project BRPR CT96 0275 is also greatly appreciated.

Appendix A. Mathematical model

A.1. Reactant balances: evolution of the kinetics

The material balance for the monomers is given by

$$\frac{dM_i}{dt} = F_i - V_w \bar{k}_{pi}^{w} [M_i]_w R_w - \bar{k}_{pi}^{p} [M_i]_p \frac{\bar{n} N_p}{N_A} \quad (A.1)$$

where M_i is the number of moles of monomer i in the reactor, F_i is its feed rate; V_w is the volume of the aqueous phase; $\bar{k}_{pi}^{z}$ is the average rate constant for propagation to monomer i in phase z (w or p) calculated as in Refs. [27], $[M_i]_z$ its concentration in phase z, $[R_w]$ is the concentration of radicals in the aqueous phase;$\bar{n}$ is the average number of radicals per particle; N_p is the number of polymer particles; and N_A is the Avogadro's number.

Partitioning of the monomers at thermodynamic equilibrium was calculated by means of an iterative algorithm using the partition coefficients and the material balances [28,29].

CTA is too insoluble to be present in the aqueous phase, and its mass balance is

$$\frac{dT}{dt} = F_t - k_{ft} [T]_p \frac{\bar{n} N_p}{N_A} \quad (A.2)$$

where T is the number of moles of CTA in the reactor, F_t is the feed rate of CTA, k_{ft} is the average constant for chain transfer to CTA, and $[T]_p$ is the concentration of CTA in the polymer particles.

The initiator balance is

$$\frac{d[I_2]}{dt} = \frac{F_I}{V_w} - k_I [I_2] \quad (A.3)$$

where $[I_2]$ is the concentration of initiator, whose thermal decomposition rate constant is k_I, and F_I is the feed rate of initiator into the reactor.

The radicals produced by the initiator decomposition or by desorption may propagate to a nonacidic monomer (S-type monomer), or an acidic monomer (A-type monomer). Details on the material balances of the different oligoradicals present in the aqueous phase and their contribution to the

development of the average number of radicals per particle can be found elsewhere [14].

A.2. Molecular weight distribution and gel fraction

Polymerization with divinyl monomers produces highly branched polymer. In the model used in this work, the only mechanism for branching is the propagation to pendant double bonds, i.e., the contributions of mutual termination and transfer to polymer are considered negligible compared to this first process. The accurate calculation of the polymer structure requires a good description of the sol MWD and to account for the compartmentalization of radicals.

In order to describe the sol MWD, the polymer was divided in generations according to its size. The first generation (e.g., $n = 0$) was formed by linear chains. The next n_e generations were composed by polymer chains having the same number of branching points [30] (e.g., all chains in generation 4 have four branching points) and for generations higher than $n_e + 1$ the geometrical growth of Teymour and Campbell [31,32] was adopted. Polymer belonging to generations higher than n_g was considered to form gel.

The number ($\bar{M}_n$) and weight ($\bar{M}_w$) average molecular weights of the sol fraction are as follows:

$$\bar{M}_{n,sol} = \frac{\sum_{n=0}^{n_g}(Q_1(n) + Y_1(n))}{\sum_{n=0}^{n_g}(Q_0(n) + Y_0(n))} P_m \tag{A.4}$$

$$\bar{M}_{w,sol} = \frac{\sum_{n=0}^{n_g}(Q_2(n) + Y_2(n))}{\sum_{n=0}^{n_g}(Q_1(n) + Y_1(n))} P_m \tag{A.5}$$

where Q_k is the kth order moment of the chain length distribution of dead polymer of all generations, Y_k stands for the kth order moment of radicals of all generations particles (generation zero is the linear generation); P_m is the molecular weight of the monomeric unit.

The amount of gel, G_1, is the total amount of monomer that has been polymerized, but which is not present in the n_g first generations

$$G_1 = Q_1 + Y_1 - \sum_{n=0}^{n_g}(Q_1(n) + Y_1(n)) \tag{A.6}$$

where n_g is the highest generation calculated. The calculation of the moments of chain length distributions of both dead and active polymer is given in Appendix B.

Appendix B. Moments of the chain length distributions of dead and active polymer

The balances for the kth order moments of the overall chain length distribution of the dead polymer in all generations (Q_k) can be expressed as the sum of the contributions of each of the processes, s, leading to the formation of dead polymer in the particles

$$\frac{dQ_k}{dt} = \sum_s \frac{dQ_{k,s}(n)}{dt} \tag{B.1}$$

The kth order moments of the chain length distribution of dead polymer in all generations produced by the different mechanisms are:

Termination by the entry of a second radical:

$$\frac{dQ_{k,abs}}{dt} = k_a[R_w]Y_k \tag{B.2}$$

Termination by transfer to monomer and CTA:

$$\frac{dQ_{k,f}}{dt} = (k_{ft}[T]_p + k_{fm}[M]_p)Y_k \tag{B.3}$$

Termination by transfer to inhibitors in the particles:

$$\frac{dQ_{k,inhib}}{dt} = (k_{tpo}[O_2]_p + k_{TBC}[TBC]_p)Y_k \tag{B.4}$$

Propagation to PDB in inactive polymer:

$$\frac{dQ_{k,PDB}}{dt} = -\frac{k_p^* p_{DB}}{N_A} Y_k Q_{k+1} \tag{B.5}$$

where p_{DB} the overall proportion of PDBs to monomer in inactive polymer:

$$p_{DB} = \frac{[DB]_t N_A}{Q_1 + Y_1} \tag{B.6}$$

where $[DB]_t$ is the concentration of PDBs in both inactive polymer and polymeric radicals, calculated by the material balance equations (B.7) and (B.8).

The balance of PDBs has two terms; formation by entry of 20% of divinyl monomer (DM) in polymer in the required conformation, and loss by propagation of radicals to PDB

$$\frac{d[DB]_t}{dt} = 0.2[DM]_p \frac{\bar{k}_{p_{DB}} Y_0}{V_p N_A} - \frac{k_p^* Y_0 [DB]_t}{V_p N_A} \tag{B.7}$$

where $[DB]_t$ is related to the concentration of pendant double bonds in inactive polymer [DB] by

$$[DB] = [DB]_t \frac{Q_1}{Q_1 + Y_1} \tag{B.8}$$

A detailed description of the material balances of the moments of the active and inactive polymer chain length distributions as well as those for the generations can be found elsewhere [14].

The closure problem, in which the calculation of each moment requires that the next be known is resolved by the Saidel and Katz [33] approximation for the third moment

$$Q_3 = 2\frac{Q_2 Q_2}{Q_1} - \frac{Q_2 Q_1}{Q_0} \tag{B.9}$$

References

[1] G. Odian, Principles of Polymerization, Wiley, New York, 1991, p. 242.

[2] M. Nomura, M. Harada, W. Eguchi, S. Nagata, J. Appl. Polym. Sci. 16 (1972) 835.
[3] J.M. Saenz, J.M. Asua, J. Polym. Sci., Part A 33 (1995) 1511.
[4] J.R. Vega, L.M. Gugliotta, R.O. Bielsa, M.C. Brandolini, G.R. Meira, Ind. Eng. Chem. Res. 36 (1997) 1238.
[5] L. Lopez de Arbina, L.M. Gugliotta, M.J. Barandiaran, J.M. Asua, Polymer 39 (1998) 4047.
[6] M.F. Cunningham, K. Geramita, J.W. Ma, Polymer 41 (2000) 5385.
[7] B.P. Huo, J.D. Campbell, A. Penlidis, J.F. MacGregor, E. Hamielec, J. Appl. Polym. Sci. 35 (1987) 2009.
[8] T.O. Broadhead, A.E. Hamielec, J.F. MacGregor, Makromol. Chem. Suppl. 10/11 (1985) 105.
[9] A. Penlidis, J.F. MacGregor, A.E. Hamielec, J. Appl. Polym. Sci. 35 (1988) 2023.
[10] A. Penlidis, J.F. MacGregor, A.E. Hamielec, Polym. Proc. Eng. 3 (1985) 185.
[11] D.C.H. Chien, A. Penlidis, Polym. React. Eng. 2 (1994) 163.
[12] D.C.H. Chien, A. Penlidis, Chem. Eng. Sci. 49 (1994) 1855.
[13] C. Kiparissides, D.S. Achilias, C.E. Frantzikinakis, Ind. Eng. Chem. Res. 41 (2002) 3097.
[14] M. Zubitur, P.D. Armitage, S. Ben Amor, J.R. Leiza, J.M. Asua, Polym. React. Eng., in press.
[15] C. Bauer, B. Amram, M. Agnely, D. Charmot, J. Sawatzki, N. Dupuy, J. Huvenne, Appl. Spectrosc. 54 (2000) 528.
[16] M. Buback, R.G. Gilbert, R.A. Hutchinson, B. Klumperman, F.D. Kuchta, B.G. Manders, K.F. O'Driscoll, G.T. Rusell, J. Schweer, Macromol. Chem. Phys. 196 (1995) 3267.
[17] D. Charmot, J.F. D'Allest, F. Dobler, Polymer 37 (1996) 5237.
[18] Rhodia, Internal communication.
[19] J.R. Richards, J.P. Congalidis, R.G. Gilbert, J. Appl. Polym. Sci. 37 (1989) 2727.
[20] X. Yuan, Ph.D. Dissertation, Lehigh University, 1996.
[21] M.A. Dube, A. Penlidis, R.K. Mutha, W.R. Cluett, Ind. Eng. Chem. Res. 34 (1996) 4434.
[22] J.A. Nelder, R. Mead, Comput. J. 7 (1964) 308.
[23] M.V. Smoluchowski, Z. Physik. Chem. 92 (1917) 129.
[24] J. Brandrup, E.H. Immergut, Polymer Handbook, 3rd ed., Wiley/Interscience, New York, 1989.
[25] R. Battino, Oxygen and Ozone, IUPAC Solubility Data Series, Pergamon Press, New York, 1981, p. 16.
[26] G. Odian, Principles of Polymerization, Wiley, New York, 1991, p. 451.
[27] J. Forcada, J.M. Asua, J. Polym. Sci., Polym. Chem. Ed. 23 (1985) 1955.
[28] S. Omi, K. Kushibiki, M. Negishi, M. Iso, Zairyo Gijutzu 3 (1985) 426.
[29] A. Urretabizkaia, G. Arzamendi, J.M. Asua, Chem. Eng. Sci. 47 (1992) 2579.
[30] G. Arzamendi, J.M. Asua, Macromolecules 28 (1995) 7479.
[31] F. Teymour, J. Campbell, DECHEMA Monogr. 127 (1992).
[32] F. Teymour, J.D. Campbell, Macromolecules 27 (1994) 2460.
[33] G.M. Saidel, S. Katz, J. Polym. Sci., Polym. Phys. 6 (1968) 1149.